AN ACCURATE AND EFFICIENT ERROR PREDICTOR TOOL FOR CATR MEASUREMENTS

Cecilia Cappellin, Stig B. Sørensen
TICRA, Læderstræde 34
1201 Copenhagen, Denmark

Maurice Paquay, Allan Ostergaard
ESTEC, European Space Research and Technology Centre, Keplerlaan 1
2201 Noordwijk, The Netherlands

ABSTRACT

An accurate and efficient numerical model is developed to simulate the far field of an antenna under test (AUT) measured in a Compact Antenna Test Range (CATR), on the basis of the known quiet zone field and the theoretical aperture field distribution of the AUT. The comparison with the theoretical far-field pattern of the AUT shows the expected measurement accuracy. The numerical model takes into account the relative movement of the AUT within the quiet zone and is valid for any CATR and AUT of which the quiet zone and aperture field, respectively, are known.
The antenna under test is the Validation Standard Antenna (VAST12), especially designed in the past for antenna test ranges validations. Simulated results as well as real measurements data are provided.

Keywords: CATR measurements, error estimation.

1. Introduction

Compact Antenna Test Ranges are widely used measurement facilities for antenna gain and pattern measurements. When measured in receive mode, the antenna under test is illuminated by a known incident quasi-planar wave, called quiet zone field, generated by the single or double reflector system of the CATR. Besides a well-designed feed for the frequency range of interest and very accurate reflector surfaces with effective serrations, CATR measurements have the big advantage of not needing probe correction and near-to-far field transformation, as is the case for spherical, cylindrical or planar near-field antenna measurements. This apparently advantageous characteristic is, however, one of the major drawbacks of CATR systems, due to the lack of a well-defined procedure to evaluate the accuracy of the measured AUT pattern.
It is well known that an antenna pattern measured in a CATR is the result of the interaction between the AUT aperture field and the field distribution in the quiet zone of the CATR, see Figure 1. Under ideal conditions, the quiet zone field distribution is a perfect plane wave with uniform amplitude and phase. In practice, the quality of the feed, the diffraction from the edges of the reflectors and the non-perfect absorbers in the facility introduce ripples in the uniform distribution of the quiet zone field, which affect the measured AUT pattern.

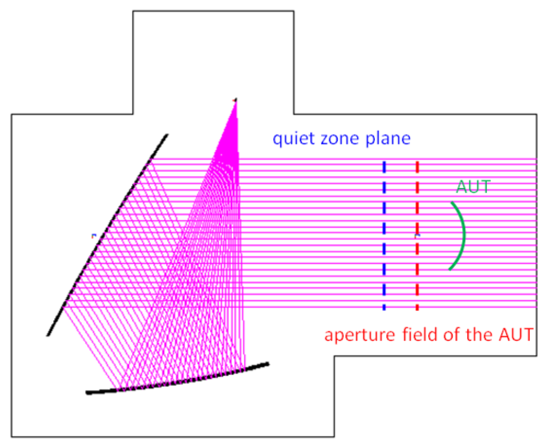

Figure 1- A typical CATR with the quiet zone field and the AUT aperture field highlighted.

Several studies have been conducted in the past with the aim at modeling the quiet zone imperfections and estimate its influence on the measured AUT field. The computation of the quiet zone field by pure Physical Optics (PO) and linear weighting of the currents over the serrated area of the CATR reflectors was presented by Jensen in 1999, [1]. The modeling of the currents over the serrated area was later improved [2] by taking into account the detailed geometry of the serrations. The effect of a non ideal quiet zone field on the AUT measured pattern was calculated by the coupling between the PO currents on the CATR reflectors and the AUT. The comparison between the AUT pattern obtained by coupling analysis and the ideal simulated pattern clearly showed the effect of the diffraction from the serrations at the angles where the AUT main beam intercepted the reflector edges. This effect, which is the main source of error in CATR measurements, was also observed and studied in detail by

Philippakis [3] by developing a 3D model of the coupling between the AUT and the CATR quiet zone. The work was based on the coupling equation involving the plane wave spectra of the AUT and the CATR, but was applied only to analytical CATR and AUT distributions and was simplified to a 2D version, due to computational reasons. Though simple in its mathematical form and already presented in [4], the coupling equation requires both an efficient algorithm to be solved, in order to make the computation of practical use, and a good knowledge of the coupling phenomena in order to discriminate between the possible sources of errors.

The purpose of this work is to develop an accurate, general and efficient numerical model, called CATREP, able to compute the expected measurement accuracy of a CATR range, on the basis of a known field in the quiet zone and a known aperture field distribution of the AUT, see Figure 1. The model is based on the coupling equation and will take into account the relative movement of the AUT within the quiet zone field. The tool will take advantage of the latest and highly efficient routines developed by TICRA during its long experience in software development, and will allow for the input and output data the well known GRASP format or the newly defined and standardized EDI format [5]. More specifically, CATREP will read as input the quiet zone distribution and the AUT aperture field, and compute the ideal far-field of the AUT and the coupling between the AUT and the CATR in the far-field region, which corresponds to the AUT pattern which is expected to be measured in the CATR. From the comparison of the theoretical antenna far-field pattern and the pattern predicted by the computational tool, the measurement accuracy of the CATR will be assessed.

The paper is organized as follows: in Section 2 the coupling theory is briefly summarized and the proposed algorithm is described, in Section 3 the approach is applied to the Validation Standard Antenna (VAST12) illuminated by an ideal and uniform quiet zone field, while in Section 4 the technique is validated by real measurement data.

2. The CATREP algorithm: theory, implementation and working principles

The mutual coupling between two antennas arbitrarily oriented and separated in free space has been studied in detail in the past, see for example the exhaustive treatment contained in [6]. Considerations and suggestions for an efficient computation are given in [4], while an alternative derivation based on the antenna as a multiport circuit can be found in [7].

The mutual coupling between two antennas, one transmitting and one receiving, is given by the so called coupling integral, and is based on the dot product and successive integration of the far fields of the two antennas. In its most general form, the coupling integral is expressed by

$$a_{rec}^{-} = -\frac{|\alpha_r|}{2k^2\zeta\sqrt{P_{rec}}}\int_{\Omega}\bar{E}_{far,rec}(\bar{k})\cdot\bar{E}_{far,trans}(-\bar{k})e^{-j\bar{k}\cdot\bar{r}}d\omega \quad (1)$$

with k being the wavenumber, $\bar{k}$ the propagation vector $\bar{k} = k\sin\theta\cos\phi\hat{x} + k\sin\theta\sin\phi\hat{y} + k\cos\theta\hat{z}$ and ζ the free space impedance. The hemisphere expressed in function of the traditional $\theta\phi$ spherical coordinates is Ω, while P_{rec} is the power of the pattern of the receiving antenna. The quantity α_r constitutes the mismatch factor of the transmitting antenna, i.e. $1-|\alpha_r|^2 = |\Gamma|^2$, where Γ is the reflection coefficient at the input antenna ports. Since this quantity depends on the underlying antenna circuit, the factor will be neglected from now on. By considering the CATR receiving and the AUT transmitting, Eq. 1 can be rewritten as

$$a_{CATR}^{-} = -\frac{1}{2k^2\zeta\sqrt{4\pi}}\int_{\Omega}\bar{E}_{far,CATR}(\bar{k})\cdot \bar{E}_{far,AUT}(-\bar{k})e^{-j\bar{k}\cdot\bar{r}_0}d\omega \quad (2)$$

It is noted that due to reciprocity, the role of the receiving and transmitting antenna can be interchanged, and that in Eq. 2 both patterns are assumed to be normalized to a total power of 4π watt, such that the output $|a_{CATR}^{-}|^2$ is the power received by the CATR when the AUT radiates a power of 4π watt. The signal a_{CATR}^{-} is the complex coupling pattern. It represents the AUT pattern measured in the CATR and is a function of the scanning grid coordinates. The vector $\bar{r}_0$ goes from the origin of the CATR coordinate system to the origin of the AUT coordinate system as illustrated in Figure 2. In order to compute Eq. 2, the CATR is assumed to be fixed in space, whereas the AUT is rotated on the given scanning grid, and for each AUT orientation the integral is computed. It is noted that to perform the integral of Eq. 2, the far-field patterns of the AUT and CATR must be expressed in the same coordinate system. Four spherical scanning grids are possible: $\theta\phi$, *uv*, Elevation over Azimuth and Azimuth over Elevation. They are all centered at the origin of the AUT coordinate system. The output obtained by CATREP is then decomposed on two polarization unit vectors. For linear polarization, they can be given by the traditional spherical unit vectors $\hat{\theta}$ and $\hat{\phi}$ or by the co- and cross-polar unit vectors $\hat{e}_{co}$ and $\hat{e}_{cx}$ according to Ludwig's third definition.

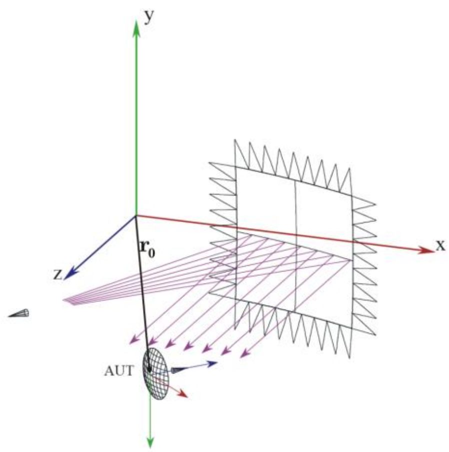

Figure 2 – Coupling between the CATR and the AUT: AUT and CATR coordinate systems.

The far-field patterns of the AUT and CATR are computed from the respective aperture fields $\bar{E}_a$, which are input to CATREP, through the corresponding equivalent magnetic currents $\bar{J}_m$

$$\bar{J}_m = -2\hat{z} \times \bar{E}_a \quad (3)$$

and the radiation integral [7]

$$\bar{E}_{far} = \frac{jk^2}{4\pi}\hat{r} \times \iint_a \bar{J}_m e^{jk(xu+yv)} dxdy \quad (4)$$

where the integral is calculated over the aperture plane and $u = \sin\theta\cos\phi$, $v = \sin\theta\sin\phi$, with $\theta\phi$ describing the forward hemisphere. The radiation from these currents represents the antenna radiation provided that the field outside the aperture plane is negligible. The integration grid in the solid angle variable $d\omega$ can be a fixed grid in which the field $\bar{E}_{far,CATR}(\bar{k})$ needs only to be calculated once, while for each output value the AUT is rotated and the $\bar{E}_{far,AUT}(\bar{k})$ is calculated at new points. To obtain a fast algorithm, expanding the aperture field in a Fourier series and computing analytically the far-field from the Fourier coefficients was found to be the most successful approach.

In the practical evaluation of Eq. 2, the integration is carried out in the CATR coordinate system and the solid angle element $d\omega$ is expressed as $d\omega = \sin\theta d\theta d\phi$. In order to save computation time for high frequencies, it is possible to reduce the half hemisphere integration domain Ω to a number of disjoint intervals $[\theta_{sn};\theta_{en}]$, which represent the areas where the significant contributions to the integral come from. The first interval is normally chosen as $[0;\theta_m]$, where θ_m includes the main beam and the first sidelobes of the CATR pattern. The next intervals should be chosen such that they capture the edge diffracted rays from the CATR main reflector rim at the angles where the AUT main beam intercepts the reflector edges. These intervals of width $\theta_e - \theta_s$ correspond to stationary points in the coupling integral and must be wide enough to contain the main lobe and first sidelobes of the AUT. It was found that $\theta_m \approx 20\lambda / D_{CATR}$, with D_{CATR} being the CATR main reflector dimension and $\theta_e - \theta_s \approx 15\lambda / D_{AUT}$, where D_{AUT} is the physical dimension of the AUT, constitute a good rule of thumb. The directions of the diffracted rays depend on the rim of the CATR main reflector and the distance between the CATR main reflector and the AUT: these can be found once the measurement set-up is known, see Figure 3. The variable ϕ has the traditional [0:2π] domain.

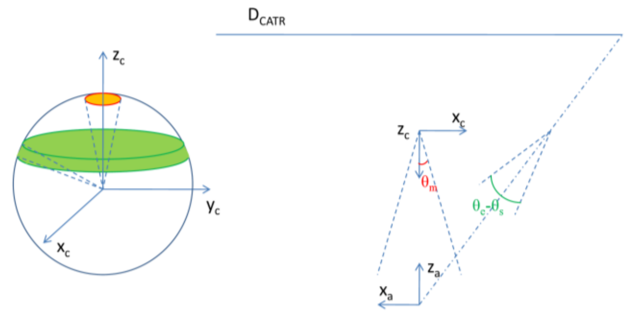

Figure 3 – Disjoint intervals in the CATR coordinate system $x_cy_cz_c$ to which the integration in the half hemisphere can be reduced: on the left in 3D, on the right in 2D.

3. Simulated results

A simple CATR quiet zone distribution was first considered. It was assumed that the CATR quiet zone field corresponded to the field radiated by a reflector of 7 by 5 meters, in the horizontal and vertical direction respectively, uniformly distributed in amplitude and phase. The origin of the CATR coordinate system $x_cy_cz_c$ was located at the center of the reflector, with *x*-axis horizontal and *y*-axis vertical, see Figure 4, in such a way that the quiet field distribution coincided with the z_c=0 plane. The AUT was constituted by the VAST12 antenna, see Figure 5. It consists of an offset shaped paraboloid working at 12 GHz, with circular projected aperture of diameter $D \approx 49$ cm $\approx 20\lambda$, and a rigid mounting structure. The antenna was designed in the nineties with the purpose of providing a stiff, robust and lightweight antenna with a number of interesting electrical properties, challenging and general enough to be tested in different measurement facilities [9].

A model of the VAST12 antenna was made with GRASP and the field radiated by the antenna was computed on the 120cm x 120cm plane located at *d*=51 cm from the center of the reflector, see Figure 6, with physical optics on the reflector and method of moments on the mounting structure and the external surface of the feed horn.

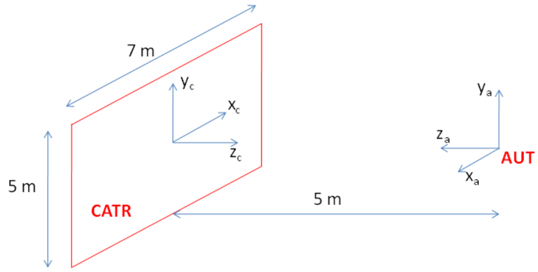

Figure 4 – CATR main reflector, the coordinate system $x_c y_c z_c$ and the AUT coordinate system $x_a y_a z_a$.

Figure 5 – The VAST12 antenna.

A plot of the obtained *y*-component is given in Figure 7. It is noted that the $x_a y_a z_a$ coordinate system depicted in Figure 6 coincides with one shown in Figure 4.

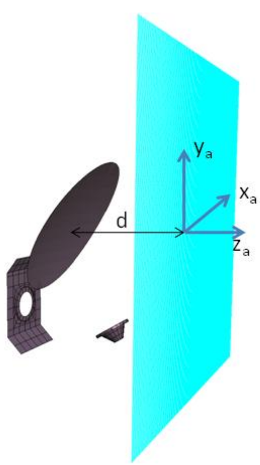

Figure 6 – GRASP model of the VAST12 antenna and the aperture plane where the field is computed.

The uniform field of the CATR at z_c=0 and the VAST12 antenna aperture field at z_a=0 were thus read by CATREP and the ideal far-field and the coupling between the antenna and the CATR in the far-field region were computed.

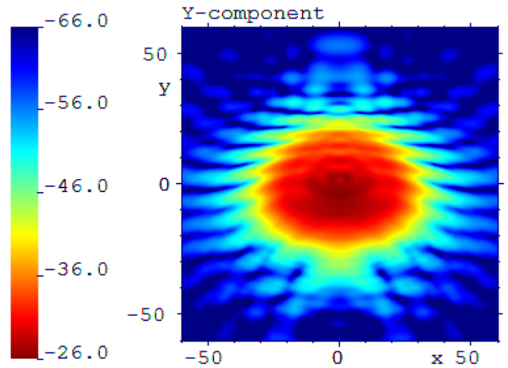

Figure 7 – Amplitude of the *y*-component of the VAST12 antenna field on the aperture plane of Figure 6.

Results can be seen in Figure 8, for the amplitude of the co- and cross-polar components in dB on the two cuts ϕ=0˚, 90˚. The upper plot refers to the case in which the CATR quiet zone is linearly polarized along x_c, while the lower plot to a quiet zone linearly polarized along y_c. It can be seen that, for both CATR polarizations, the co-polar components on the two phi-cuts of the coupling pattern coincide with the expected far-field in the main lobe and sidelobes except for a clear diffraction effect which occurs around the angles where the AUT main lobe intercepts the CATR rim, i.e. at $\theta \approx 35$˚for ϕ=0˚ and at $\theta \approx 26.5$˚for ϕ=90˚. The cross-polar component, which does not exist for ϕ=90˚, is affected by the same diffraction, but to a lower degree.

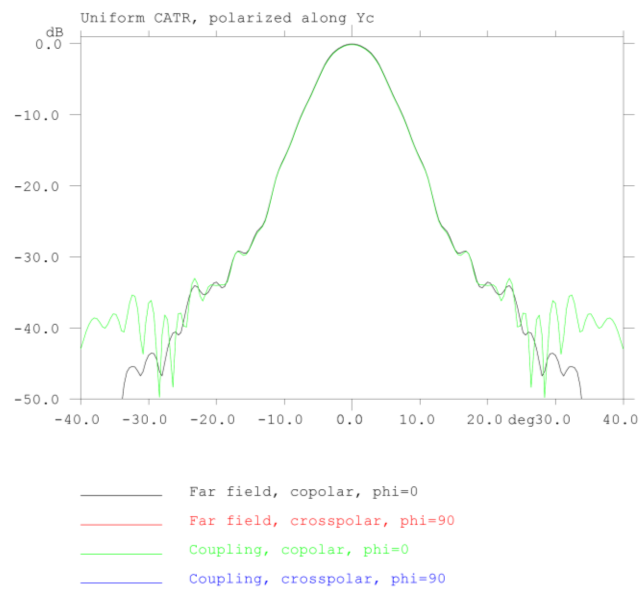

Figure 8 – Amplitude of the far-field and coupling pattern for a uniform CATR distribution and the VAST12 antenna.

4. Experimental results

The quiet zone field distribution was then given by the field distribution measured in the ESTEC CPTR (Compact Payload Test Range), see Figure 9 for a plot of the amplitude of the x-component. It is noted that only the x-component of the quiet zone field was available, while the y-component was assumed to be zero. It is reminded that such a quiet zone field distribution only describes the quiet zone field of the CPTR in a circular area of 1 m radius, see Figure 9, corresponding to the size of the mirror used to perform the quiet zone measurement. In practice the quiet zone field distribution of the ESTEC CPTR has a radius almost one meter wider.

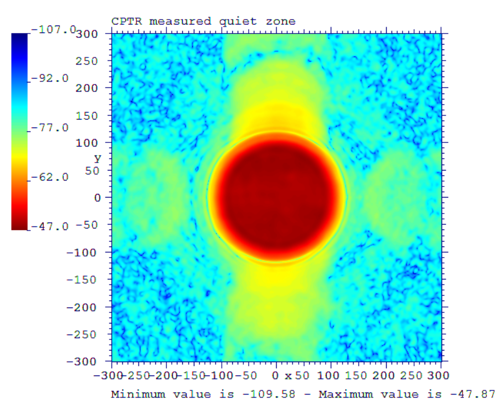

Figure 9 - Amplitude of the *x*-component of the quiet zone field measured in the CPTR, (*xy*-plane in cm).

The CPTR geometry is shown in Figure 10. The main reflector has a dimension of 8800 mm x 7500 mm, including serrations, where D_{CATR}=8800 mm. The distance d between the centre of the main reflector and the origin of the quiet zone coordinate system is d=17777 mm. The VAST12 coordinate system $x_a y_a z_a$ is oriented as in Figure 6 but the origin is displaced from the center of the aperture. The distance between the origin of the VAST12 and CPTR coordinate systems is equal to d_2=274.125 mm

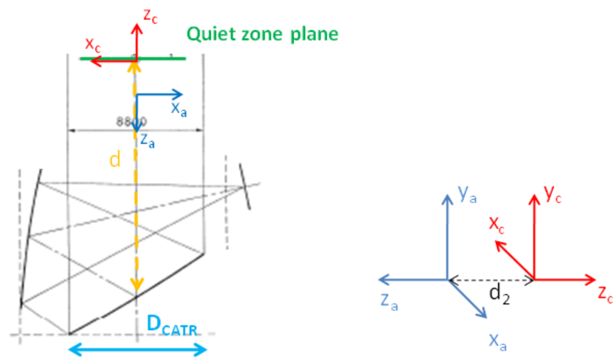

Figure 10 – CPTR geometry (the distance between the coordinate systems is not to scale), and the VAST12 $x_a y_a z_a$ and CPTR $x_c y_c z_c$ coordinate systems.

The obtained patterns are shown in Figure 11, normalized to their maxima. It can be seen that the cross-polar component at φ=0° of the far-field computed from the VAST12 aperture field coincides with the coupling cross-polar component. The far-field component is perfectly symmetric, while the coupling one shows an almost unnoticeable asymmetry. The co-polar component on φ=90° shows very good agreement in the main lobe, while sidelobes of the ideal far-field are in general higher than the ones of the coupling pattern. This is particularly evident in the first two sidelobes for theta around -8° and in the first one for theta almost 8°. The co-polar component for φ=0° of the far-field, not shown here, coincides with the coupling one in the ±10° theta range, while for theta smaller than 0°the coupling sidelobes are generally higher. This does not happen for theta larger than 0°, where they mainly coincide.

The obtained patterns can be compared to the coupling patterns shown in Figure 8 for a uniform quiet zone field distribution. Though the distance between the AUT coordinate system and the rim of the CPTR reflector in Section 3 was equal to 5 m, important observations can be made. We can notice that diffraction effects exist in both coupling patterns. The diffractions are at (or close to) the angles where the AUT main beam intercepts the CPTR reflector rim. For the coupling given by the quiet zone measured by ESTEC, these angles were estimated to be around ±8°, due to the reduced size of the quiet zone field distribution. For a uniform quiet zone field and a CPTR main reflector with straight rim, the diffraction effect is highly concentrated around this defined angular direction, while its influence is smaller but more spread when a quiet zone field coming from a CPTR main reflector with serrations and tapered illumination is considered. Serrations together with the tapered illumination of the reflectors decrease the current distributions on the CPTR reflectors close to the rim, and thus the diffraction from the edges, but widen the CATR spectrum.

Figure 11 - Coupling and far-field pattern obtained by CATREP with measured quiet zone data.

7. Summary

A general, accurate and efficient numerical model was developed to simulate the far field of an antenna under test measured in a Compact Antenna Test Range, on the basis of the coupling between the known quiet zone field of the CATR and the theoretical aperture field distribution of the AUT. The model takes into account the relative movement of the AUT during the measurement process. The theory behind the numerical model was summarized and the working principles of the algorithm were explained.

The AUT was constituted by the VAST12 antenna, and its aperture field was computed with GRASP. The quiet zone field was first considered ideal and uniform, and later substituted by a measured distribution. In both cases the comparison between the ideal AUT far-field and the coupling pattern clearly showed the inaccuracies introduced by a CATR measurement, given by sidelobes errors at the angle where the AUT main beam intercepts the CPTR reflector rim. This is more evident in the co-polar than in the cross-polar pattern. These errors are significant, but concentrated in space, for a uniform quiet zone distribution; they decrease in amplitude, but spread in angular region, for a quiet zone coming from a reflector with tapered illumination and serrations.

For a detailed and accurate validation of the CATREP software, the measured quiet zone field distribution of the CPTR must be known on the complete aperture and a CPTR measurement of the VAST12 antenna must be performed.

8. REFERENCES

[1] Jensen, F., Giauffret, L., Marti-Canales, J., “Modeling of compact range quite zone fields by PO and GTD”, Proceedings of Antenna Measurements Technique Association, Symposium, AMTA, Monterey Bay, USA, pp. 242-247, October 1999.

[2] Jensen, F., Pontoppidan, K., “Modeling of the antenna-to-range coupling for a compact range”, Proceedings of Antenna Measurements Technique Association, Symposium, AMTA, Denver, CO, USA, pp. 387-391, October 2001.

[3] Philippakis, M., Parini, C. G., “Compact antenna range performance evaluation using simulated pattern measurements”, IEE Proc. Microw. Antennas Propag., Vol. 143, No. 3, June 1996, pp. 200-206..

[4] Yaghjian, A. D., “Efficient computation of antenna coupling and fields within the near-field region”, IEEE Transactions on Antennas and Propagation, Vol. AP-30, No. 1, Jan. 1982, pp. 113-128.

[5] Martinaud, J.-P., Frandsen, P.E., Vandenbosch, G., “The ACE activity on standardized file formats for electromagnetic software”, Proceedings of European Conference on Antennas and Propagation, EuCAP, 2006.

[6] Kerns, M. D., “Plane-wave scattering matrix theory of antennas and antenna-antenna interactions”, Nat. Bur. Stand. Monograph 162, June 1981.

[7] Collin, R.E., Zucker, F. J., “Antenna Theory, Part I”, McGraw Hill, 1969.

[8] Cappellin, C., Sørensen, S. B., “CATR Error Budget Predictor”, Technical note n. 2, S-1505-02, contract 22106/08/NL/ST, April 2009.

[9] Hansen, J. E., “Definition, design, manufacture, test use of a 12 GHz Validation Standard Antenna”, Technical report R672, EMI, Technical University of Denmark, October 1997.

9. ACKNOWLEDGMENTS

This work was supported by the European Space Agency under the contract number 22106/08/NL/ST.